GPS-Based Real-Time Identification of Tire–Road Friction Coefficient

Jin-Oh Hahn, Rajesh Rajamani, *Member, IEEE*, and Lee Alexander

***Abstract*—Vehicle control systems such as collision avoidance, adaptive cruise control, and automated lane-keeping systems as well as ABS and stability control systems can benefit significantly from being made "road-adaptive." The estimation of tire–road friction coefficient at the wheels allows the control algorithm in such systems to adapt to external driving conditions. This paper develops a new tire–road friction coefficient estimation algorithm based on measurements related to the lateral dynamics of the vehicle. A lateral tire force model parameterized as a function of slip angle, friction coefficient, normal force and cornering stiffness is used. A real-time parameter identification algorithm that utilizes measurements from a differential global positioning system (DGPS) system and a gyroscope is used to identify the tire–road friction coefficient and cornering stiffness parameters of the tire. The advantage of the developed algorithm is that it does not require large longitudinal slip in order to provide reliable friction estimates. Simulation studies indicate that a parameter convergence rate of 1 s can be obtained. Experiments conducted on both dry and slippery road indicate that the algorithm can work very effectively in identifying a slippery road.**

***Index Terms*—Friction identification, global positioning system (GPS), parameter identification, tire–road friction, vehicle dynamics.**

I. Introduction

OVER THE last ten years, there has been significant interest in research on intelligent vehicles and intelligent vehicle-highway systems [1]–[3]. Considerable work has been carried out on collision avoidance, collision warning, adaptive cruise control and automated lane-keeping systems as well as on ABS, stability control, and other control algorithms for emergency maneuvers. All of these vehicle control systems can benefit significantly from being made "road-adaptive," i.e., the control algorithms can be modified to account for the external driving condition of the vehicles if the tire–road friction coefficients at the wheels are available.

This paper concentrates on developing and demonstrating a reliable algorithm for tire–road friction coefficient estimation. Several tire–road friction coefficient estimation algorithms have been previously suggested in the literature [4]–[8]. However, a significant number of these algorithms depend on using wheel speeds and measurements related to vehicle longitudinal dynamics in order to estimate the friction coefficient [4]–[6]. Longitudinal slip-based algorithms require adequate longitudinal slip in order to be able to identify friction [8]. This constitutes a limitation, since longitudinal slip is typically very small for normal driving conditions. This project develops a new estimation algorithm for cornering stiffness and tire–road friction coefficient based on utilizing only the lateral dynamics of the vehicle measured using a differential global positioning system (DGPS).

Manuscript received September 5, 2000; revised May 27, 2001. Manuscript received in final form January 14, 2002. Recommended by Associate Editor M. Jankovic. This work was supported in part by the Minnesota Department of Transportation and by the ITS-Institute, University of Minnesota.

The authors are with the Department of Mechanical Engineering, University of Minnesota, Minneapolis, MN 55455 USA (e-mail: rajamani@me.umn.edu).

Publisher Item Identifier S 1063-6536(02)03418-8.

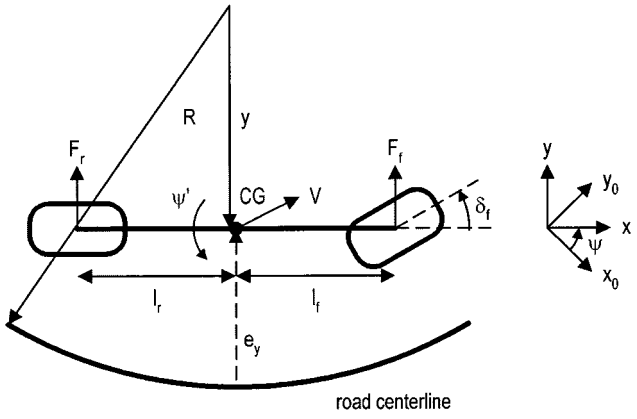

Fig. 1. Schematic diagram for lateral vehicle dynamics.

The use of GPS and DGPS for vehicle navigation and for vehicle location services has been investigated by many researchers (see, for example, [9]) and even commercialized by practitioners. The use of DGPS for vehicle control and for vehicle state estimation, however, is still a relatively new research area and some results can be found in conference presentations [10]–[12].

II. Lateral Vehicle Dynamics and Lateral Tire Force

A dynamic model for the vehicle with two degrees of freedom is considered in this paper. The two degrees of freedom are the lateral position of the center of gravity (c.g.) of the vehicle and the yaw angle of the vehicle. The lateral position y is measured along the body-fixed lateral axis of the vehicle while the yaw angle ψ is determined with respect to global coordinates (x_0, y_0) (Fig. 1).

Describing the lateral position in terms of lateral position error e_y with respect to a road reference, the dynamic model can be described by the following equations [13]:

$$m\ddot{e}_y + m\dot{\psi}_d V = F_f + F_r \tag{1a}$$

$$I_z\ddot{\psi} = l_f F_f - l_r F_r \tag{1b}$$

where e_y is the lateral distance of the vehicle c.g. from the road (or lane) reference, m is the mass of the vehicle, $\dot{\psi}_d = V/R$ is the yaw rate of the road defined by the road curvature R and the

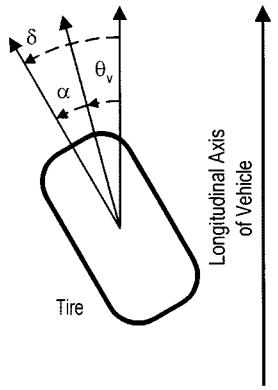

Fig. 2. Tire slip angle.

longitudinal velocity V, I_z is the yaw moment of inertia, l_f is the distance from c.g. to the front tires, l_r is the distance from c.g. to the rear tires and F_f and F_r are front and rear tire forces, respectively.

The lateral force at each tire is known to depend on the slip angle, the tire–road friction coefficient and the normal force at the tire. The slip angle α is the angle between the orientation of the tire and the orientation of the velocity vector of the wheel, and is shown in Fig. 2. Here δ is the steering angle of the wheel and θ_v is the angle of the velocity vector at the wheel.

Typical characteristics of tire force as a function of slip angle and tire–road friction coefficient are shown below in Fig. 3. The normal force is assumed to be constant. As can be seen from the figure, for a given tire–road friction coefficient, tire force initially increases with slip angle and then saturates. For very small slip angles, the force is proportional to slip angle and the proportionality constant is called the cornering stiffness. In general, the tire force increases with the tire–road friction coefficient for a given cornering stiffness, except at very small slip angles.

Assuming longitudinal slip is small, the following mathematical equation can be used to represent the tire force on the front tires [7]:

$$F_f = 2\mu F_z \left\{ \left| \frac{C_f \tan\alpha_f}{\mu F_z} \right| - \frac{1}{3} \left| \frac{C_f \tan\alpha_f}{\mu F_z} \right|^2 + \frac{1}{27} \left| \frac{C_f \tan\alpha_f}{\mu F_z} \right|^3 \right\} \operatorname{sgn}(\alpha_f), \quad \left| \frac{C_f \tan\alpha_f}{\mu F_z} \right| \le 3 \tag{2}$$

where μ is the tire–road friction coefficient, F_z is the normal force acting on each tire, C_f is the cornering stiffness of each front tire and α_f is the front tire slip angle defined by

$$\alpha_f = \delta_f - \tan^{-1}\left(\frac{\dot{e}_y - (\psi - \psi_d)V + l_f\dot{\psi}}{V} \right). \tag{3}$$

Note that the lateral velocity at the front wheels is given by $\dot{e}_y - (\psi - \psi_d)V + \ell_f\dot{\psi}$ [13].

The tire force on the rear tires is similarly defined as follows:

$$F_r = 2\mu F_z \left\{ \left| \frac{C_r \tan\alpha_r}{\mu F_z} \right| - \frac{1}{3} \left| \frac{C_r \tan\alpha_r}{\mu F_z} \right|^2 + \frac{1}{27} \left| \frac{C_r \tan\alpha_r}{\mu F_z} \right|^3 \right\} \operatorname{sgn}(\alpha_r), \quad \left| \frac{C_r \tan\alpha_r}{\mu F_z} \right| \le 3 \tag{4}$$

where C_r is the cornering stiffness of each rear tire and α_r is the rear tire slip angle defined by

$$\alpha_r = -\tan^{-1}\left(\frac{\dot{e}_y - (\psi - \psi_d)V - l_r\dot{\psi}}{V} \right). \tag{5}$$

III. Cornering Stiffness/Tire–Road Friction Coefficient Estimator Synthesis

A. Plant Parametric Model Derivation

The tire force equations (2) and (4) contain three unknown parameters of interest, i.e., the cornering stiffness C_f and C_r, and the tire–road friction coefficient μ. Generally it is not desirable to try to identify many parameters simultaneously, since the excitation signal into the system needs to be richer as the number of parameters to be identified increases. For the specific identification problem at hand, the number of parameters to be identified can be reduced to two by manipulating (1) to eliminate the rear tire force term

$$ml_r\left(\ddot{e}_y + \dot{\psi}_d V\right) + I_z\ddot{\psi} = (l_f + l_r)F_f. \tag{6}$$

Substituting (2) into (6), the following equation can be obtained:

$$\ddot{e}_y + \dot{\psi}_d V + \frac{I_z}{ml_r}\ddot{\psi} = 2\frac{l_f + l_r}{ml_r}\left\{ |C_f \tan\alpha_f| - \frac{1}{3}\frac{|C_f \tan\alpha_f|^2}{|\mu F_z|} + \frac{1}{27}\frac{|C_f \tan\alpha_f|^3}{|\mu F_z|^2} \right\} \operatorname{sgn}(\alpha_f). \tag{7}$$

Although (7) seems to be highly nonlinear, the unknown parameters can be linearly separated from the known regressor terms as follows. Define

$$z = \frac{s^2}{(s+a)^2}e_y + \frac{1}{(s+a)^2}\dot{\psi}_d V + \frac{s^2}{(s+a)^2}\frac{I_z}{ml_r}\psi \tag{8}$$

$$\Theta = [\theta_1 \quad \theta_2 \quad \theta_3]^T = \left[C_f \quad \frac{C_f^2}{\mu} \quad \frac{C_f^3}{\mu^2} \right]^T \tag{9}$$

$$\Phi = [\phi_1 \quad \phi_2 \quad \phi_3]^T = 2\frac{\operatorname{sgn}(\alpha_f)}{(s+a)^2}\frac{l_f + l_r}{ml_r} \cdot \left[|\tan\alpha_f| \quad -\frac{|\tan\alpha_f|^2}{3F_z} \quad \frac{|\tan\alpha_f|^3}{27F_z^2} \right]^T \tag{10}$$

where s denotes the Laplace transform operator and a is a filter constant to be chosen appropriately. The filter $1/(s+a)^2$ is

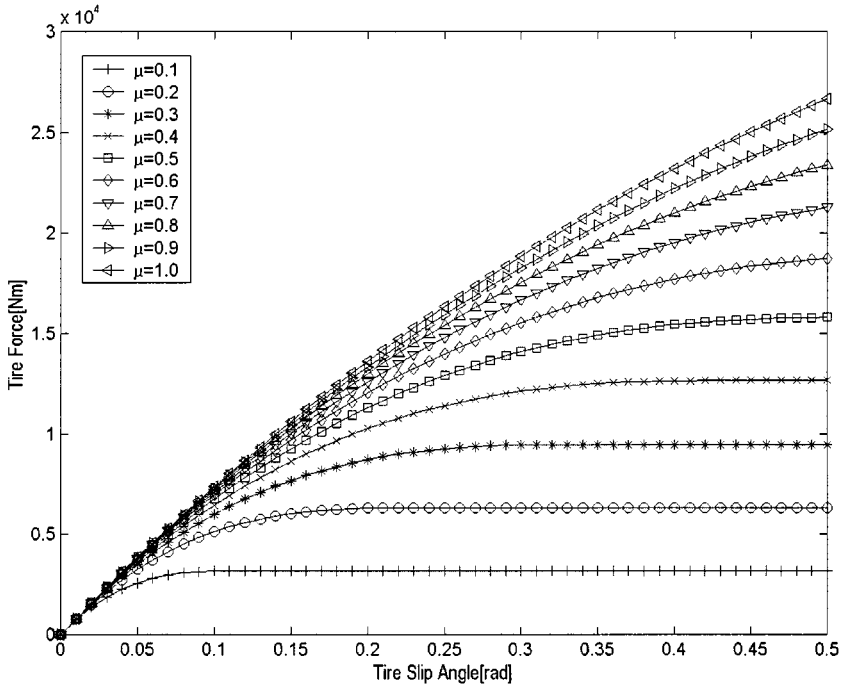

Fig. 3. Lateral tire force versus lateral slip angle.

used to ensure that the signal z is causal and can be obtained once e_y, $\dot{\psi}_d$, V and ψ are measured. The slip angle α_f can be obtained from (3) once δ_f, e_y, ψ, ψ_d and $\dot{\psi}$ are measured. Notes on measurement of the above signals in the experimental setup can be found in Section V.

Using (8)–(10), the following linear parametric model can be obtained for the system:

$$z = \Theta^T \Phi. \tag{11}$$

It is to be noted that there are two unknowns of interest, i.e., the front tire cornering stiffness C_f and the tire–road friction coefficient μ, whereas there are three parameters in the parameter vector. In other words, the parameters in the parameter vector in (9) are redundant.

So far we have assumed that the normal force F_z is known and have included it in the regressor. In practice, the normal force on the tires cannot be easily measured. The following algorithm is suggested for estimating the normal forces using the suspension dynamics. A two degrees-of-freedom quarter-car model of an automotive suspension is shown below in Fig. 4. The sprung mass m_s represents the vehicle body, the unsprung mass m_u represents the mass of the tire and axle, k and b are the stiffness and damping of the vehicle suspension and k_t and b_t are the stiffness and damping of the tire.

The equation of motion for the unsprung mass can be easily derived as follows:

$$m_u \ddot{z}_u = -b_t(\dot{z}_u - \dot{z}_r) - k_t(z_u - z_r) + b(\dot{z}_s - \dot{z}_u) + k(z_s - z_u) \tag{12}$$

where $\ddot{z}_u$ is the absolute acceleration of the unsprung mass, and $z_u - z_r$ and $z_s - z_u$ are the deflections of tire and suspension, respectively. Hence the normal force acting on the tire can be

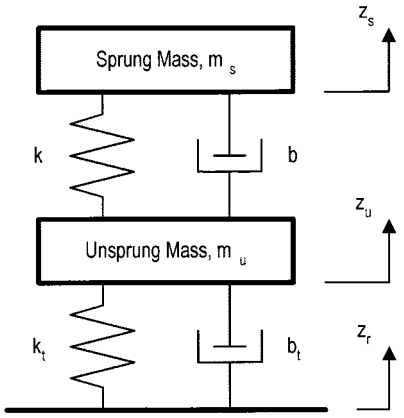

Fig. 4. Schematic diagram of an automotive suspension.

estimated by measuring $\ddot{z}_u$ and $z_s - z_u$ and using the following equation:

$$\begin{aligned} F_z &= b_t(\dot{z}_u - \dot{z}_r) + k_t(z_u - z_r) \\ &= b(\dot{z}_s - \dot{z}_u) + k(z_s - z_u) - m_u \ddot{z}_u. \end{aligned} \tag{13}$$

This is a dynamic estimator for the tire normal force F_z and differs from the static estimator presented in [14]. The estimator presented in [14] calculated the normal tire force statically (ignoring suspension dynamics) based on the vehicle weight, c.g. location, vehicle longitudinal acceleration, aerodynamic drag forces and centripetal acceleration on curves. The estimator presented above, on the other hand, calculates the normal force dynamically using the dynamic relations at each wheel. It is expected to be more accurate. Use of the estimator requires sensors that measure vertical acceleration of the axle, suspension deflection and relative suspension velocity. While accelerometers are very inexpensive, the measurement

of suspension deflection and velocity is a more expensive proposition.

B. Estimator Synthesis

As pointed out above, the parameters θ_1, θ_2 and θ_3 in (9) are redundant, i.e., they are interrelated to one another as follows:

$$\theta_3 = \frac{\theta_2^2}{\theta_1}. \tag{14}$$

For the parametric model in (11), define the following estimated signal:

$$\hat{z} = \hat{\Theta}^T \Phi = [\,\hat{\theta}_1 \quad \hat{\theta}_2 \quad \hat{\theta}_3\,]\,\Phi \tag{15}$$

where $\hat{z}$ is the estimate for the output signal of the parametric model and $\hat{\theta}_1$, $\hat{\theta}_2$ and $\hat{\theta}_3$ are the estimates for the unknown parameters θ_1, θ_2 and θ_3, respectively.

The standard methodology to obtain a parametric identification adaptive law for the plant model in (11) is as follows. Based on (11) and (15), the steepest descent algorithm [15]–[17] can be used to derive the adaptive law:

$$\dot{\hat{\theta}}_1 = \gamma_1 \varepsilon \phi_1,\ \dot{\hat{\theta}}_2 = \gamma_2 \varepsilon \phi_2,\ \dot{\hat{\theta}}_3 = \gamma_3 \varepsilon \phi_3,\ \varepsilon = \frac{z - \hat{z}}{\sqrt{1 + \Phi^T \Phi}} \tag{16}$$

where γ_1, γ_2 and γ_3 are adaptive gains, and ε is the normalized output estimation error.

Here, it should be noted that the parameters θ_1, θ_2 and θ_3 are estimated as if they were independent of one another. Unless we have persistence of excitation that can ensure convergence of all three parameters, it would be impossible to uniquely determine the cornering stiffness and the tire–road friction coefficient. This drawback will be demonstrated later with simulation results.

To overcome the aforementioned difficulty and uniquely determine the cornering stiffness and the tire–road friction coefficient, an approximated estimator utilizing the parameter redundancy is synthesized in this paper. Expanding the estimated output signal, the estimated signal can be manipulated into the following two-dimensional regressor form:

$$\begin{aligned}\hat{z} &= \hat{\Theta}^T \Phi \\ &= \hat{\theta}_1 \phi_1 + \hat{\theta}_2 \phi_2 + \hat{\theta}_3 \phi_3 \\ &= \hat{\theta}_1 \phi_1 + \hat{\theta}_2 \phi_2 + \hat{\theta}_3 \frac{|\tan \alpha_f|^2}{27 F_z^2} \phi_1 \\ &= \hat{\vartheta} \phi_1 + \hat{\theta}_2 \phi_2 \\ &= [\,\hat{\vartheta} \quad \hat{\theta}_2\,]\,\varphi\end{aligned} \tag{17}$$

where $\hat{\vartheta}$ is defined as follows:

$$\hat{\vartheta} = \hat{\theta}_1 + \frac{|\tan \alpha_f|^2}{27 F_z^2} \hat{\theta}_3 = \hat{\theta}_1 + \frac{|\tan \alpha_f|^2}{27 F_z^2} \frac{\hat{\theta}_2^2}{\hat{\theta}_1}. \tag{18}$$

Then the following adaptive law can be obtained using the conventional ordinary gradient algorithm:

$$\dot{\hat{\vartheta}} = \gamma_\vartheta \varepsilon \phi_1, \quad \dot{\hat{\theta}}_2 = \gamma_2 \varepsilon \phi_2, \quad \varepsilon = \frac{z - \hat{z}}{\sqrt{1 + \Phi^T \Phi}} \tag{19}$$

where γ_ϑ and γ_2 are adaptive gains, and ε is the normalized output estimation error. Now it is straightforward to show that the output estimation error will converge to zero, and the parameters $\hat{\vartheta}$ and $\hat{\theta}_2$ will converge to the true values if the regressor vector φ satisfies the persistent excitation requirement.

Unfortunately, the parameters cannot be uniquely determined if the above adaptive law is used without modification since the following second-order equation, which is directly derived from the definition of $\hat{\vartheta}$, has to be solved at each time step to determine the value of $\hat{\theta}_1$, which generally has two distinct roots

$$\hat{\theta}_1^2 - \hat{\vartheta} \hat{\theta}_1 + \frac{|\tan \alpha_f|^2}{27 F_z^2} \hat{\theta}_2^2 = 0. \tag{20}$$

To solve this drawback, the approximate adaptive law for $\hat{\vartheta}$ is derived as follows. From the definition of $\hat{\vartheta}$

$$\begin{aligned}\dot{\hat{\vartheta}} &= \gamma_\vartheta \varepsilon \phi_1 \\ &= \dot{\hat{\theta}}_1 + \frac{d}{dt}\left(\frac{|\tan \alpha_f|^2}{27 F_z^2} \hat{\theta}_3\right) \\ &= \dot{\hat{\theta}}_1 + \frac{|\tan \alpha_f|^2}{27 F_z^2} \dot{\hat{\theta}}_3\end{aligned} \tag{21}$$

where the term $|\tan \alpha_f|^2 / 27 F_z^2$ is considered as a given quantity at every time step since it can be explicitly calculated using the measured signals. It is also noted that this simplification dramatically facilitates the derivation of the approximated adaptive law (without this assumption, we can not derive an adaptive law of the form $\gamma \varepsilon \phi$). From the redundancy relation for $\hat{\theta}_3$, i.e., $\hat{\theta}_3 = \hat{\theta}_2^2 / \hat{\theta}_1$, the time derivative of $\hat{\theta}_3$ is given by

$$\dot{\hat{\theta}}_3 = \frac{2 \hat{\theta}_1 \hat{\theta}_2 \dot{\hat{\theta}}_2 - \hat{\theta}_2^2 \dot{\hat{\theta}}_1}{\hat{\theta}_1^2}. \tag{22}$$

Substituting (22) into (21), and rearranging with respect to $\dot{\hat{\theta}}_1$

$$\begin{aligned}\dot{\hat{\theta}}_1 \left(1 - \frac{|\tan \alpha_f|^2}{27 F_z^2} \frac{\hat{\theta}_2^2}{\hat{\theta}_1^2}\right) &= \gamma_\vartheta \varepsilon \phi_1 - 2 \frac{|\tan \alpha_f|^2}{27 F_z^2} \frac{\hat{\theta}_2}{\hat{\theta}_1} \dot{\hat{\theta}}_2 \\ &= \gamma_\vartheta \varepsilon \phi_1 + 2 \frac{|\tan \alpha_f|^3}{81 F_z^3} \frac{\hat{\theta}_2}{\hat{\theta}_1} \gamma_2 \varepsilon \phi_1\end{aligned} \tag{23}$$

from which the following adaptive law is derived for $\hat{\theta}_1$:

$$\begin{aligned}\dot{\hat{\theta}}_1 &= \left(1 - \frac{|\tan \alpha_f|^2}{27 F_z^2} \frac{\hat{\theta}_2^2}{\hat{\theta}_1^2}\right)^{-1} \left(\gamma_\vartheta + 2 \frac{|\tan \alpha_f|^3}{81 F_z^3} \frac{\hat{\theta}_2}{\hat{\theta}_1} \gamma_2\right) \varepsilon \phi_1 \\ &= \gamma_{11}\left(\hat{\theta}_1, \hat{\theta}_2, \alpha_f\right) \gamma_{12}\left(\hat{\theta}_1, \hat{\theta}_2, \gamma_\vartheta, \gamma_2, \alpha_f\right) \varepsilon \phi_1.\end{aligned} \tag{24}$$

Thus, the adaptive law for $\hat{\theta}_1$ has been derived as the same form as the ordinary gradient algorithm with time varying adaptive gain. Regarding the sign of the adaptive gain, it can be argued that the sign of the gain γ_{12} can be kept positive by appropriate choice of the gains γ_ϑ and γ_2 such that the parameter estimates $\hat{\vartheta}$ and $\hat{\theta}_2$ assume positive values and the determinant in (25) holds, which is obvious from (20). It in turn implies that the sign of the adaptive gain for $\hat{\theta}_1$ is dominated by γ_{11}

$$\hat{\vartheta}^2 - \frac{4 |\tan \alpha_f|^2}{27 F_z^2} \hat{\theta}_2^2 \geq 0. \tag{25}$$

Further simplification can be made to the adaptive law for $\hat{\theta}_1$ if the adaptive gain is selected as constant with switching sign, that is

$$\dot{\hat{\theta}}_1 = \mathrm{sgn}(\gamma_{11})\gamma_1 \varepsilon \phi_1. \tag{26}$$

Summarizing the above discussion, the following approximated adaptive law for the unknown parameters θ_1, θ_2 and θ_3 has been derived, where γ_1 is some positive constant:

$$\dot{\hat{\theta}}_1 = \mathrm{sgn}(\gamma_{11})\gamma_1 \varepsilon \phi_1, \quad \dot{\hat{\theta}}_2 = \gamma_2 \varepsilon \phi_2, \quad \hat{\theta}_3 = \frac{\hat{\theta}_2^2}{\hat{\theta}_1}. \tag{27}$$

It is also noted from (24) that the gain γ_{11} is positive for slip angles that are not extremely large, which is usually the case in real situations. The adaptive law in (27) is an approximation to the actual adaptive law in (19) and the adaptive gain for $\hat{\theta}_1$ may not be optimal since the gain has been simplified to a constant version. In spite of that, unknown parameters can be uniquely determined using the adaptive law in (27), in contrast to the actual adaptive law in (19).

Comparing (27) to the ordinary gradient algorithm in (16), which does not take the parameter redundancy into account, it can be argued that the proposed adaptive law is more efficient than the ordinary gradient algorithm from the persistence of excitation point of view. This is because the proposed adaptive law is based upon a two-dimensional regressor vector, whereas the ordinary gradient algorithm in (16) is based upon a three-dimensional one, for which it is harder to satisfy the persistence of excitation requirement.

IV. Extension to Operation Under Combined Traction and Cornering

The tire force models described by (2) and (4) are valid under the assumption of small longitudinal slip [7]. Longitudinal slip can be defined as follows:

$$\sigma_x = 1 - \frac{\Omega_0}{\Omega} \tag{28}$$

where Ω is the wheel speed of revolution and

$$\Omega_0 = \frac{V}{r_e} \tag{29}$$

is obtained from the translational speed of the wheel, with r_e being the effective tire radius and V the vehicle velocity.

In the case where longitudinal slip is significant (for instance, during hard braking on a slippery surface), the lateral force generated by a tire would be less than that obtained from the expressions (2) and (4). The lateral force model can, however, be modified for combined traction/cornering while still retaining the same structure and the same parameters in the model.

Define the lateral slip as

$$\sigma_y = \frac{\Omega_0}{\Omega} \tan\alpha \tag{30}$$

where α is the slip angle as defined earlier in (3) and (5). The total slip can then be defined as

$$\sigma = \sqrt{\sigma_x^2 + \sigma_y^2} \tag{31}$$

and is composed of the lateral and longitudinal slip.

Define the scalar variable

$$F = 2\mu F_z \left\{ \frac{C_f \sigma}{\mu F_z} - \frac{1}{3}\left(\frac{C_f \sigma}{\mu F_z}\right)^2 + \frac{1}{27}\left(\frac{C_f \sigma}{\mu F_z}\right)^3 \right\} \quad \text{if } \frac{C_f \sigma}{\mu F_z} \le 3 \tag{32}$$

$$F = 2\mu F_z \quad \text{if } \frac{C_f \sigma}{\mu F_z} > 3. \tag{33}$$

The longitudinal and lateral forces at each set of tires (front or rear) can then be obtained as

$$F_x = \frac{\sigma_x}{\sigma} F \tag{34}$$

$$F_y = \frac{\sigma_y}{\sigma} F \tag{35}$$

respectively.

Note that the lateral force defined by (32) and (35) has exactly the same functional structure as that in (2) and (4). In fact the parameters involved are the same friction coefficient μ and cornering stiffness C_f. The exactly same estimator as described in Section III can therefore be used for the combined traction/cornering problem. The only change required is in the lateral tire force model and involves calculation of the total slip and the calculation of the lateral portion of the tire force using the ratio $F_y = (\sigma_y/\sigma)F$.

The calculation of the total slip requires measurement of individual wheel speeds. These measurements were unavailable on our experimental vehicle. The simulation and experimental results described in the following sections therefore demonstrate the working of the algorithm under pure "cornering only" operation.

Note that even in the case of combined traction/cornering, *the lateral vehicle dynamics* will be used to calculate friction in the methodology described in this paper. The fundamental idea presented in the paper and the estimation algorithm will thus not change even for combined traction/braking and cornering.

At this stage, a few comments on the accuracy of the above combined lateral–longitudinal tire model are in order. The model assumes a Coulomb friction coefficient. In reality, the friction coefficient does depend on the slip speed as well as on the normal force, tire pressure, and temperature [18]. In addition, the model assumes the same lateral and longitudinal tire stiffness. The lateral and longitudinal tire stiffness can however differ, by as much as a factor of 1 : 2. A relatively more complex empirical model that addresses the above limitations has been suggested in [18]. The use of a more accurate tire model (to improve estimator accuracy) could be a topic for future research.

It should also be noted that the estimation algorithm assumes that the values of mass m and inertia I_z are known. An online measurement/estimation method for the variables would be valuable. For instance, monitoring the static suspension deflections at all tire locations or monitoring the tire pressure at all locations could be used to obtain estimates of mass, c.g. location, and vehicle inertia.

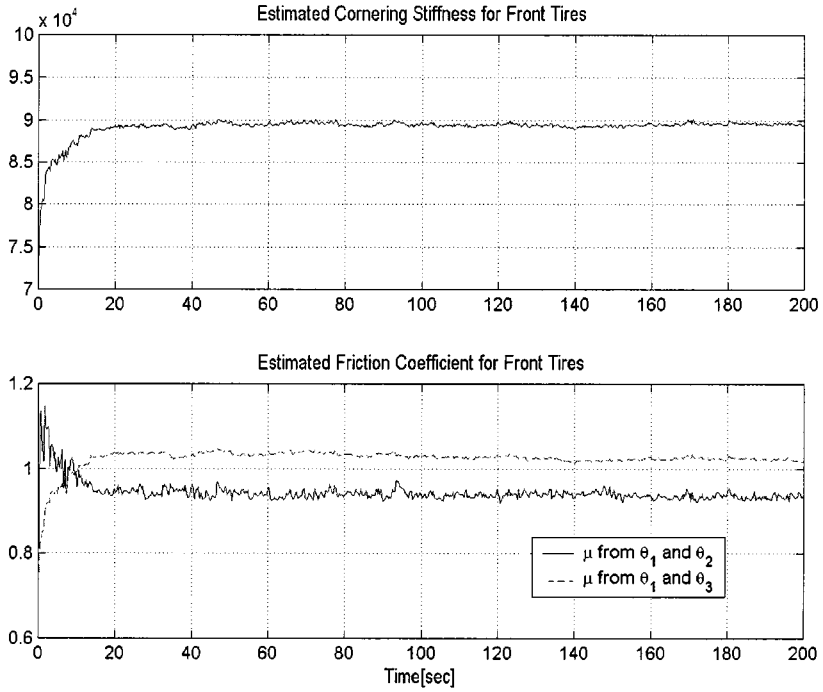

Fig. 5. Parameter convergence with ordinary adaptive law.

V. Simulation Studies

The properties, performance, and limitations of the proposed parameter identification algorithm are investigated through intensive simulation studies. The simulation model used is the fourth-order model described in (1)–(5).

A. Comparison of Standard and Proposed Adaptive Laws

The parameter convergence trajectories for the standard adaptive law and the proposed new adaptive law are compared in Figs. 5 and 6. The true cornering stiffness and tire–road friction coefficient are assumed to be 90 000 N/rad and 0.9, respectively, and random noise with zero mean and 0.02 variance has been used as the steering input signal. In this simulation it is illustrated that tire–road friction coefficient cannot be uniquely determined with the standard adaptive law.

From Fig. 5, we see that the friction coefficient estimate converges to either 1.05 or 0.95 depending on whether $\hat{\theta}_1$ and $\hat{\theta}_2$ or $\hat{\theta}_1$ and $\hat{\theta}_3$ is used for the estimation in the standard adaptation law.

From Fig. 6, we see that the modified identification algorithm correctly yields a friction estimate of 0.9.

B. Influence of Slip Angle and Underlying Friction Coefficient on Parameter Convergence

The effect of the magnitude of the slip angle on the accuracy of tire–road friction coefficient identification is illustrated in Fig. 7. In the simulation of Fig. 7, sinusoids of $\delta(t) = M \sin 0.5\pi t$ rad with $M = 0.2$, 0.1, 0.03 and $V(t) = 15$ m/s are used for the steering input signal and the longitudinal velocity signal, respectively. The true tire–road friction coefficient is assumed to be 0.9, and the cornering stiffness has been set to exact value in the simulation to clearly show the effect of the slip angle magnitude on the tire–road friction coefficient estimate. The corresponding maximum slip angles for the front tires turn out to be 0.14 rad, 0.07 rad, and 0.02 rad, respectively, from simulation. It is noticed that the accuracy of the tire–road friction coefficient estimate becomes worse as the slip angle magnitude becomes smaller. This phenomenon can be explained by the tire force curve shown in Fig. 3. It can be seen in Fig. 3 that tire–road friction coefficient does not play a significant role in the region where the slip angle is very small because tire force curves are almost the same regardless of the values of the tire–road friction coefficient in that region. This in turn implies that in real situations it is hard to identify the tire–road friction coefficient if the tire slip angle generated by the steering and longitudinal velocity signals is too small.

However, an important point to be noted is that as the friction coefficient becomes smaller, the lateral tire force is influenced by the fiction coefficient at smaller and smaller slip angles. Consider the lateral tire force in (2). At small slip angles and large friction coefficients, the terms

$$\frac{1}{3}\left|\frac{C_f \tan\alpha_f}{\mu F_z}\right|^2 \quad \text{and} \quad \frac{1}{27}\left|\frac{C_f \tan\alpha_f}{\mu F_z}\right|^3$$

can be neglected so that the tire force is approximately $F_f = 2C_f\alpha_f$ and is independent of the friction coefficient. However, at small friction coefficients, these terms are no longer negligible, even if the slip angle is small. Thus smaller friction coefficients can be more easily identified even with smaller slip angles.

The above conclusion can also be obtained by analyzing the results of previous researchers. Consider the Gough plot shown in Fig. 8. The utilized friction potential [7] is defined by

$$\mu_u = \frac{F_f}{2\mu F_z}. \tag{36}$$

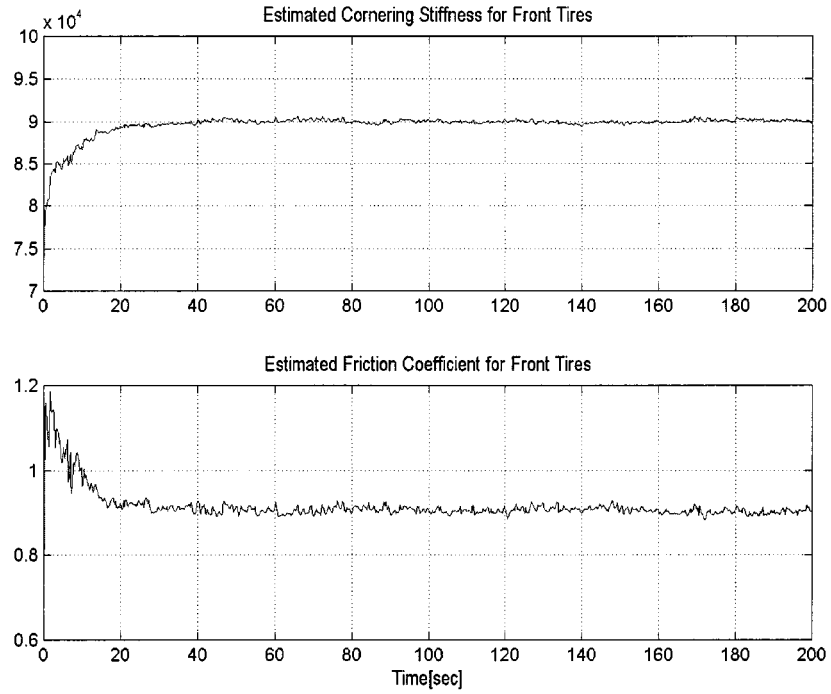

Fig. 6. Parameter convergence with proposed adaptive law.

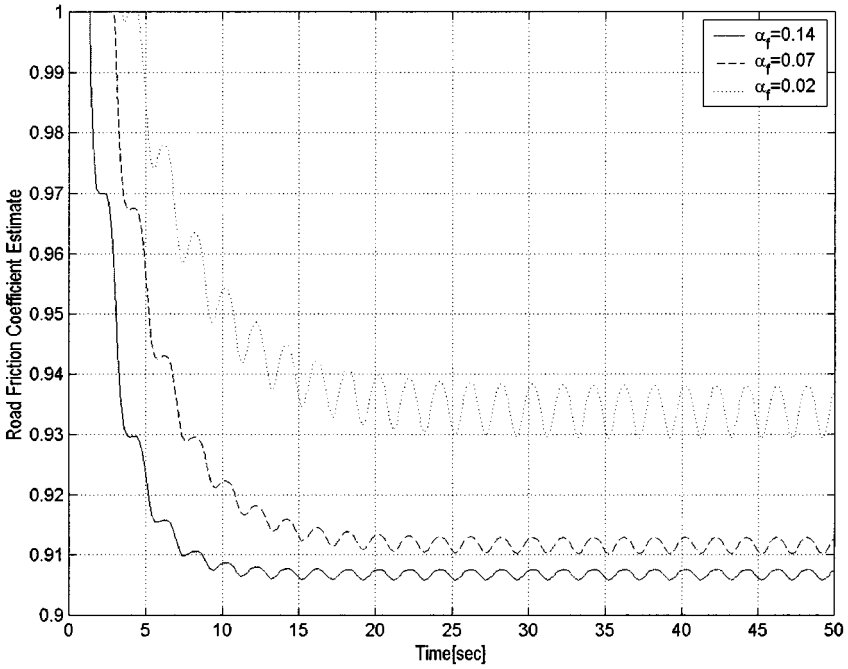

Fig. 7. Accuracy of tire–road friction coefficient estimate with respect to slip angle magnitudes.

Physically, it implies the actually used lateral tire force of a tire divided by the maximum possible tire force that can be generated by the tire under the given tire–road friction coefficient. It has been reported in Pasterkamp and Pacejka [7], while evaluating a neural-network algorithm for friction identification, that it is hard to exactly identify the tire–road friction coefficient for small values of μ_u. In accordance with this fact, it can be easily seen using the Gough plot shown in Fig. 8 that the estimator will require large slip angle to get large μ_u and reasonably exact parameter estimates for the case with large tire–road friction coefficient. In contrast to the large tire–road friction coefficient case, smaller slip angle will be enough to obtain sufficiently large μ_u for the case with small tire–road friction coefficient, which is also evident from the Gough plot in Fig. 8. Because the magnitude of the required slip angle is directly related to how severe the lateral vehicle maneuver should be, it can be stated that a mild lateral vehicle maneuver will be enough to identify a small tire–road friction coefficient. On the other hand, a more severe lateral vehicle maneuver will be required to identify a large tire–road friction coefficient.

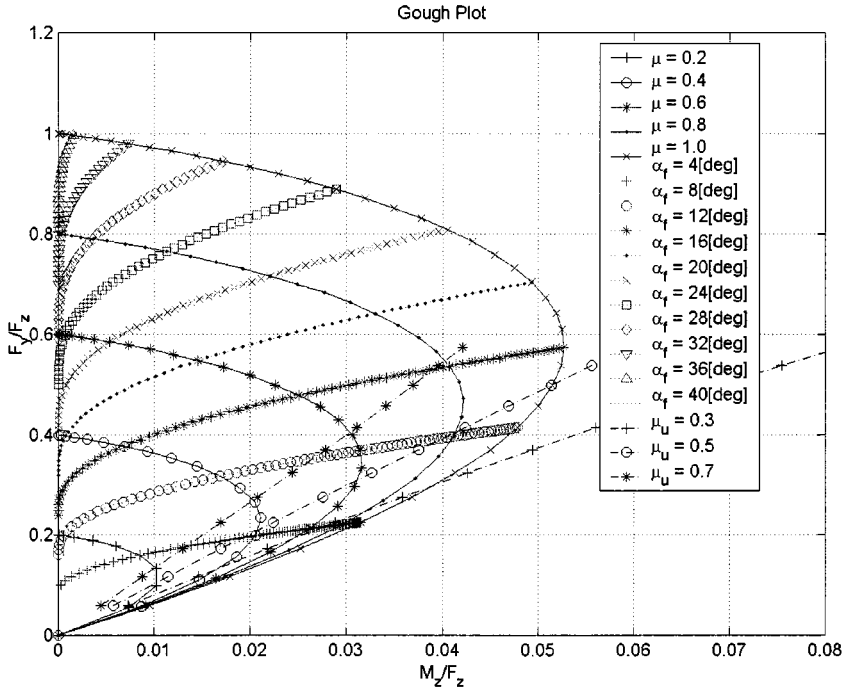

Fig. 8. Gough plot for the tire.

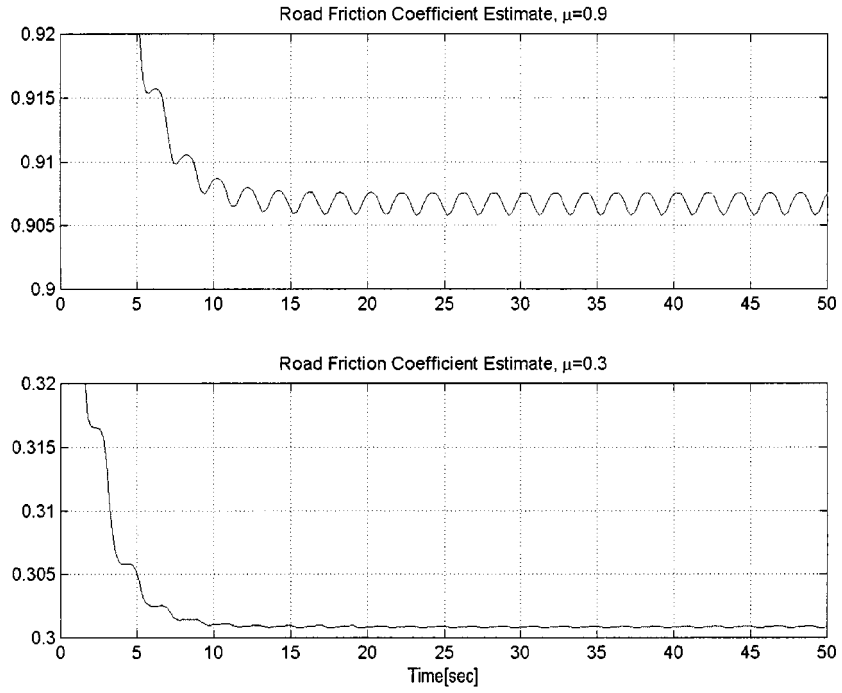

Fig. 9. Accuracy of tire–road friction coefficient estimate for different tire–road friction coefficients.

The above argument is justified by the simulation result shown in Fig. 9, where the same steering input and longitudinal velocity signals are applied to a vehicle on the road with $\mu = 0.9$ and $\mu = 0.3$, respectively. As can be seen from the simulation result, the steady-state estimation error for the tire–road friction coefficient is smaller by about ten times for the case with $\mu = 0.3$ than the case with $\mu = 0.9$.

Summarizing the above discussion, it can be concluded that the estimator will not work well for extremely small slip angles. But this is the inherent characteristic of the system under consideration, and similar results will be obtained even if other algorithms are applied to the problem at hand, assuming that the algorithm is based only upon the lateral vehicle maneuver. In addition, it is also shown that it is easier to identify parameters in case the underlying tire–road friction coefficient is small, since it becomes easier to generate sufficiently large μ_u as the tire–road friction coefficient becomes smaller.

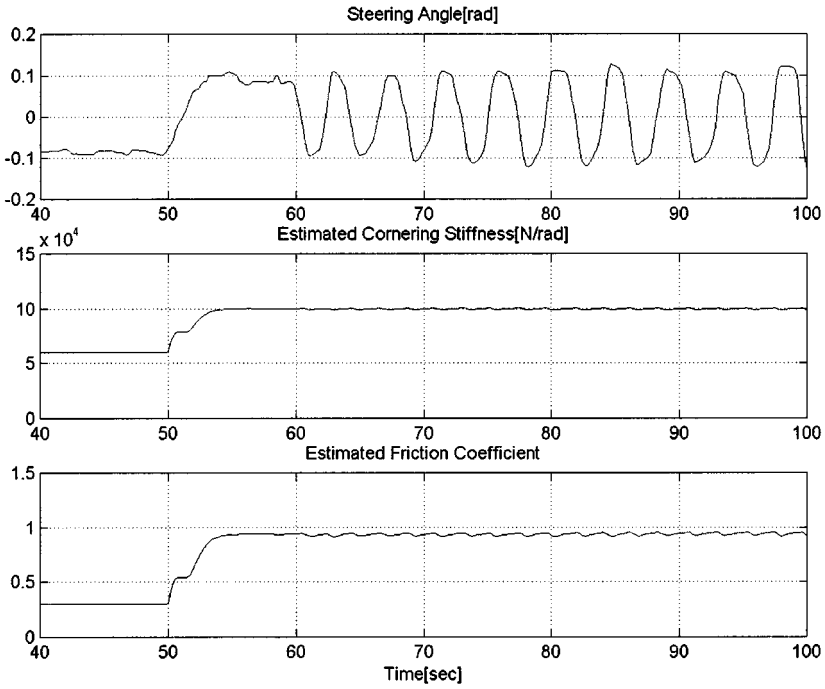

Fig. 10. Parameter identification simulation: dry road.

C. Ideal Simulation With Experimental Steering and Longitudinal Velocity Input Signals

To evaluate the performance of the cornering stiffness and tire–road friction coefficient identification algorithm in an ideal noise-free situation, experimental steering and longitudinal velocity input signals are used in a simulation study. The experimental signals serve as inputs to a simulation model which generates the trajectories for the states of the model.

A dry road with friction coefficient of 0.9 is assumed first. The underlying cornering stiffness is assumed to be 100 000 N/rad. The steering input used is shown in Fig. 10. The identified cornering stiffness and tire–road friction coefficient parameters are shown in the same figure. The longitudinal velocity is about 10 m/s. It can be seen that the estimator returns the parameter estimates with good accuracy and also that the rate of parameter convergence is about 1.5 s.

The identified cornering stiffness and tire–road friction coefficient for slippery road surface in a similar noise-free situation are demonstrated in Fig. 11. The longitudinal velocity is less than 10 m/s. The underlying cornering stiffness and tire–road friction coefficient are assumed to be 70 000 N/rad and 0.3, respectively. The rate of convergence of approximately 1 s has been achieved for the ideal parameter identification on slippery road with excellent accuracy for the parameter estimates. This result is in line with our claim that the proposed tire–road friction identification algorithm is useful for the detection of slippery road surfaces.

VI. Experimental Results

The parameter identification algorithm was implemented on a 9400 Navistar truck equipped with a differential GPS system, a gyroscope and a steering angle sensor. The experimental setup is described in Section VI-A. Experiments were carried out both on dry and slippery roads to evaluate the real-time efficacy of the identification algorithm.

A. Experimental Setup

The Navistar 9400 tractor cab used for the experiments is shown in Fig. 12. Though the figure shows a tractor-trailer, only the tractor was used for this experimental work. The truck is front wheel drive and is equipped with a Novatel RT-20 GPS system aided by differential correction. The Novatel RT-20 is known to provide an accuracy of 20 cm with on-the-fly initialization. However, for our application, the GPS system was found to provide the position of the truck to an accuracy of 2.5 cm at an update rate of 200 ms. The better accuracy was due to static initialization of the system and due to the close distance of the reference station from the experimental tests. In addition, an Andrews fiber-optic gyroscope was used to measure the yaw rate of the truck and a potentiometer on the steering wheel column was used to measure the steering angle. The tire–road friction coefficient and cornering stiffness identification algorithm was implemented using the RT Kernel operating system on a PC laptop.

B. Calculation of Lateral Position Error e_y

The differential GPS signals can be used to calculate the absolute position (x, y) of the vehicle with respect to a global coordinate axes. However, the parameter identification algorithm has been obtained assuming measurement of the lateral position error e_y with respect to a road reference. This lateral position error e_y is calculated from the GPS measurement (x, y) as follows. Consider the vehicle and the road as shown in Fig. 13. It is easy to show that the following equations are satisfied in Fig. 13:

$$\tan(-\psi) = \frac{x - x_r}{y - y_r} \tag{37}$$

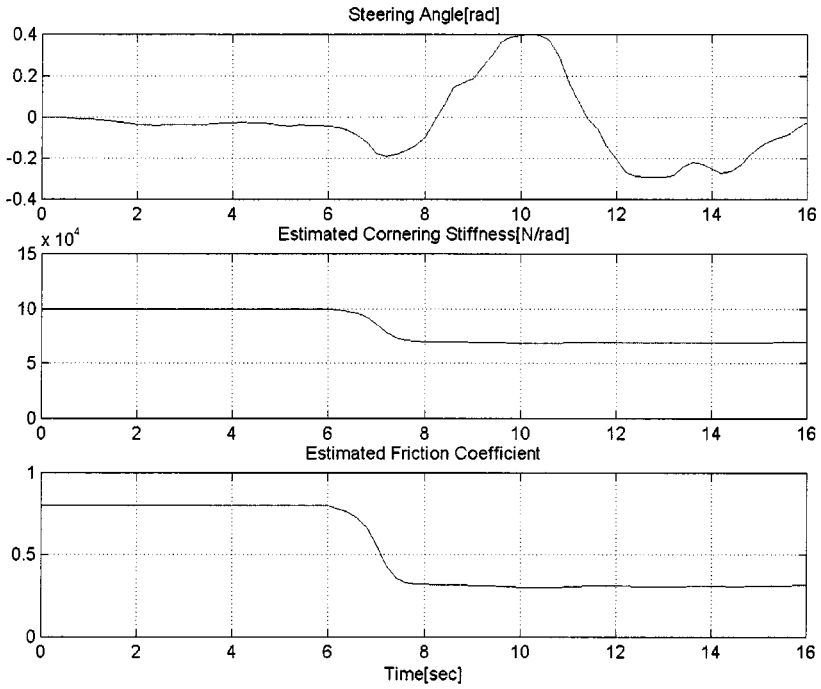

Fig. 11. Parameter identification simulation: slippery road.

Fig. 12. Navistar 9400 tractor-trailer.

$$\frac{x_r - x_{r1}}{y_r - y_{r1}} = \frac{x_{r2} - x_{r1}}{y_{r2} - y_{r1}} \tag{38}$$

where (x, y) is the vehicle GPS position, (x_{r1}, y_{r1}) and (x_{r2}, y_{r2}) are any two known points on the road and (x_r, y_r) is the desired vehicle position.

The equations in (37) and (38) can be solved for (x_r, y_r). Once (x_r, y_r) is obtained, the lateral position error e_y is defined by the distance between (x_r, y_r) and (x, y)

$$e_y = \operatorname{sgn}(y - y_r)\operatorname{sgn}(\cos\psi)\sqrt{(x - x_r)^2 + (y - y_r)^2}. \tag{39}$$

Derivation of the sign for e_y shown in (39) is tedious but straightforward [19].

The points (x_{r1}, y_{r1}) and (x_{r2}, y_{r2}) on the road are obtained as follows. The GPS locations of regularly spaced points on the road are stored in a database as a geographic map. The database is then accessed in real time and the reference points closest to the vehicle are obtained. Such geographic databases containing road reference points are expected to be widely available very soon for the entire country. The preparation of a statewide geographic database for highways is underway in Minnesota.

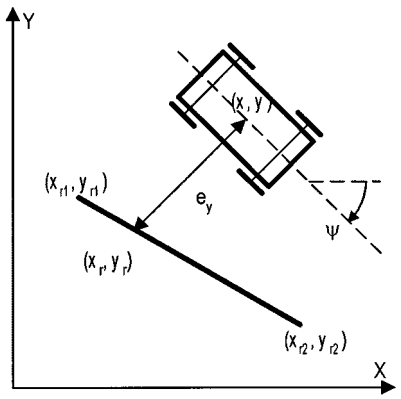

Fig. 13. Calculation of lateral position error based on GPS signals.

The variables necessary for the calculation of slip angles in (3) and (5) include the yaw rate $\dot{\psi}$, the yaw angle ψ, the desired angle ψ_d, the vehicle speed V and the steering angle δ_f. The desired yaw angle is the angle of the line between the points (x_{r1}, y_{r1}) and (x_{r2}, y_{r2}) and can also be obtained from the road database. The yaw angle of the vehicle can be obtained from GPS signals using

$$\psi_{\mathrm{GPS}} = \tan^{-1}\left(\frac{\dot{y}}{\dot{x}}\right). \tag{40}$$

However, $\dot{y}$ and $\dot{x}$ in (40) have to both be obtained by numerical differentiation making this a very noisy signal. The yaw angle can also be obtained by integrating the yaw rate signal measured

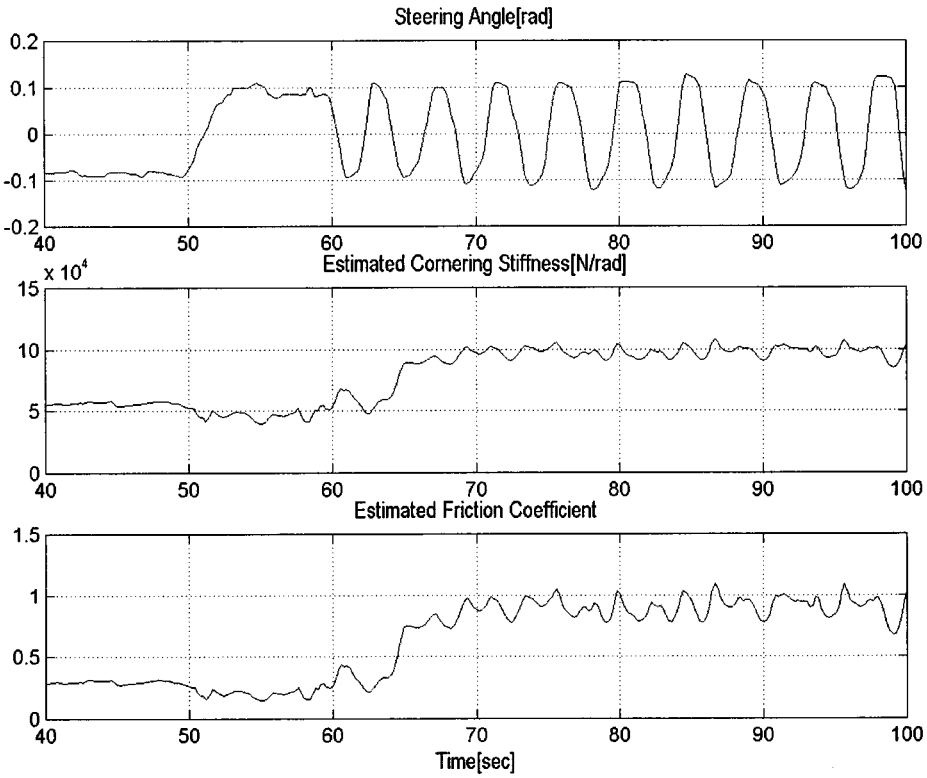

Fig. 14. Parameter identification result: dry road.

by a gyroscope $\dot{\psi}_{\text{gyro}}$. However, the signal obtained by integration of the yaw rate usually drifts due to bias errors present in the yaw rate signal. The following observer that utilizes both the gyroscope and GPS is therefore used to obtain ψ:

$$\dot{\hat{\psi}} = \dot{\psi}_{\text{gyro}} + k\left(\psi_{\text{GPS}} - \hat{\psi}\right). \tag{41}$$

Here the term $\psi_{\text{GPS}} - \hat{\psi}$ corrects for the drift that occurs when the gyroscope signal $\dot{\psi}_{\text{gyro}}$ is integrated. If the gyroscope signal were perfect with no bias errors, then there would be no drift and the use of GPS would be unnecessary. A very small value of k leads to a slow correction in drift but a smoother signal. A high value of k leads to a quicker correction of drift but a noisier estimate.

All other variables required for calculation of slip angle from (3) are measured and available.

Based on the measurement requirements, note that the friction estimation algorithm presented in this paper can be used not only for automated highway applications but also for other evolutionary applications on today's highways. The necessary elements for the use of the algorithm are a lateral position measurement system and a road database. Differential GPS and GPS- based databases are both likely to be available on a widespread basis in the next few years.

C. Experimental Results

The efficacy of the algorithm to identify friction on a dry road has been tested using numerous steering excitation profiles. A steering excitation consisting of a weaving motion while driving on a straight road is shown in Fig. 14. The identified cornering stiffness and tire–road friction coefficient are also illustrated in the same figure. The longitudinal velocity is about 10 m/s. It can be seen that the proposed tire–road friction identification algorithm works well in the presence of the above lane-change-type maneuvers. Although the underlying cornering stiffness and the tire–road friction coefficient are not exactly known, the estimates in this experiment are very reasonable.

Experiments were also conducted on a skid pad at a police training ground, which provided a slippery surface. The steering excitation used is shown in Fig. 15. It consists of a quick lane change followed by another lane change back into the same lane. This steering maneuver results in lateral slip and some loss of steering control by the driver. There was no braking during the maneuver. The identified cornering stiffness and tire–road friction coefficient are illustrated in Fig. 15. The longitudinal velocity is less than 10 m/s. It can be seen that both cornering stiffness and the tire–road friction coefficient converge to reasonable values, although there exist oscillations in both estimates. The oscillations are expected to be due to normal force variations in the tires and due to inaccuracies in the tire force model. The friction coefficient estimate of 0.4 provided by the algorithm seems appropriate. The vehicle used for the skid pad experiments was a snow-plow and differs from the Navistar tractor-trailer described earlier. It had smaller tires than the Navistar tractor-cab. This can be used to describe the difference in the estimated value of the cornering stiffness.

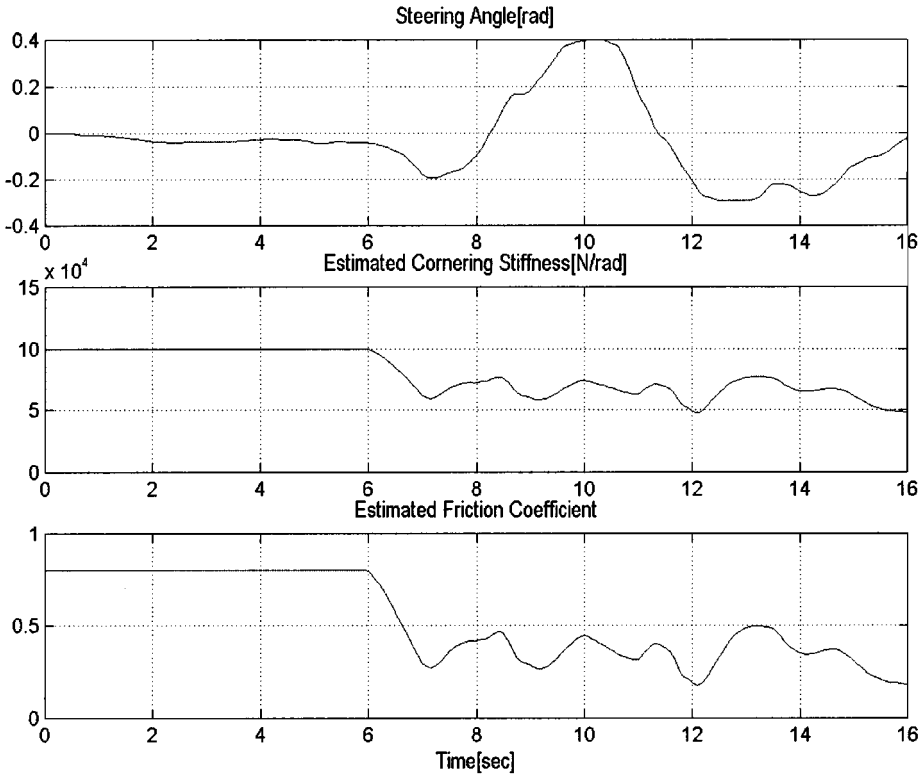

Fig. 15. Parameter identification result: slippery road.

VII. Conclusion

This paper developed and investigated a new tire–road friction coefficient estimation algorithm based on measurements related to the lateral dynamics of the vehicle. A lateral tire force model applicable over a wide range of slip-angles was used. An innovative parameter identification algorithm utilized measurements from a differential GPS system and a gyroscope to identify the friction coefficient and cornering stiffness parameters of the tire. Experiments conducted on both dry and slippery road indicated that the algorithm worked very effectively in identifying the friction coefficient. The algorithm was able to provide a time constant of 1 s for real-time convergence of the friction coefficient estimate.

An inherent limitation of using the lateral dynamics to identify friction coefficient is that the identification algorithm cannot work well if the slip angles generated by the excitation are very small. Results in the paper, however, showed that the algorithm would still be effective at distinguishing a slippery road from a dry road. This happens because the performance of the identification algorithm keeps improving as the friction coefficient decreases, even if the slip angle remains small.

The advantage of the developed algorithm is that it does not require large longitudinal slip in order to provide reliable friction estimates. The algorithm would be useful in providing road-adaptability to vehicle control systems such as collision avoidance, adaptive cruise control, and automated lane-keeping systems as well as ABS and stability control systems.

Acknowledgment

The authors would like to express their appreciation to J. Scharffbillig from the Minnesota Department of Transportation for the help provided in driving the snow plow for the skid-pad tests described in this paper.

References

[1] R. Rajamani, S. B. Choi, J. K. Hedrick, B. K. Law, R. Prohaska, and P. Kretz, "Design and experimental implementation of longitudinal control for a platoon of automated vehicles," *ASME J. Dynamic Syst., Measurement, Contr.*, vol. 122, pp. 470–476, Sept. 2000.

[2] J. Guldner, H. S. Tan, and S. Patwardhan, "Analysis of automatic steering control for highway vehicles with look-down lateral reference systems," *Veh. Syst. Dynamics*, vol. 26, pp. 243–269, Oct. 1996.

[3] Y. Zeyada, D. Karnopp, M. El-Arabi, and E. El-Behiry, "A combined active-steering differential braking yaw rate control strategy for emergency maneuvers," in *Proc. SAE 980230*, 1998.

[4] F. Gustafsson, "Monitoring tire–road friction using the wheel slip," *IEEE Contr. Syst. Mag.*, vol. 18, pp. 42–49, Aug. 1998.

[5] K. Yi and T. Jeong, "Observer based estimation of tire–road friction for collision warning algorithm adaptation," *JSME Int. J. (C)*, vol. 41, pp. 116–124, Mar. 1998.

[6] H. Nishira, T. Kawabe, and S. Seiichi, "Road friction estimation using adaptive observer with periodical σ-modification," in *Proc. IEEE Int. Conf. Contr. Applicat.*, 1999, pp. 662–667.

[7] W. R. Pasterkamp and H. B. Pacejka, "The tire as a sensor to estimate friction," *Vehicle Syst. Dyn.*, vol. 27, pp. 409–422, June 1997.

[8] L. R. Ray, "Nonlinear tire force estimation and road friction identification: Simulation and experiments," *Automatica*, vol. 33, pp. 1819–1833, Oct. 1997.

[9] J. Farrell, T. Givargis, and M. Barth, "Differential carrier phase GPS-aided INS for automotive applications," in *Proc. Amer. Contr. Conf.*, 1999, pp. 3660–3664.

[10] D. M. Bevly, J. C. Gerdes, C. Wilson, and G. Zhang, "The use of GPS based velocity measurements for improved vehicle state estimation," in *Proc. Amer. Contr. Conf.*, 2000, pp. 2538–2542.

[11] L. Wang, T. Emura, and T. Ushiwata, "Automatic guidance of a vehicle based on DGPS and a 3D map," in *Proc. IEEE Conf. Intell. Transportation Syst.*, 2000, pp. 131–136.
[12] L. Alexander and M. Donath, "Differential GPS based control of a heavy vehicle," in *Proc. IEEE Conf. Intell. Transportation Syst.*, 1999, pp. 662–667.
[13] H. Peng and M. Tomizuka, "Preview control for vehicle lateral guidance in highway automation," *ASME J. Dynamic Syst., Measurement, Contr.*, vol. 115, pp. 678–686, Dec. 1993.
[14] F. Gustafsson, "Slip-based tire–road friction estimation," *Automatica*, vol. 33, pp. 1087–1099, June 1997.
[15] S. Sastry and M. Bodson, *Adaptive Systems: Stability, Convergence and Robustness*. Englewood Cliffs, NJ: Prentice-Hall, 1989.
[16] P. A. Ioannou and J. Sun, *Robust Adaptive Control*. Englewood Cliffs, NJ: Prentice-Hall, 1996.
[17] K. J. Astrom and B. Wittenmark, *Adaptive Control*. Reading, MA: Addison-Wesley, 1988.
[18] H. B. Pacejka and R. S. Sharp, "Shear force development by pneumatic tires in steady state conditions: A review of modeling aspects," *Veh. Syst. Dynamics*, vol. 20, no. 3–4, pp. 121–176, 1991.
[19] C. Zhu, "GPS-based automated parking," M.S. thesis, Dept. Mech. Eng., Univ. Minnesota, Minneapolis, 2000.

Jin-Oh Hahn received the B.S. and M.S. degrees from the Department of Mechanical Design and Production Engineering, Seoul National University, Korea, in 1997 and 1999, respectively.

He is currently an Instructor in the Department of Mechanical Engineering, Korea Air Force Academy, Korea. His research interests include control design, state estimation, failure identification, and reconfigurable control for advanced vehicle control systems.

Rajesh Rajamani (M'94) received the B.Tech degree from the Indian Institute of Technology at Madras in 1989 and the M.S. and Ph.D. degrees from the University of California, Berkeley, in 1991 and 1993, respectively.

He was a Research Engineer at United Technologies Research Center (UTRC) from 1993 to 1996. From August 1996 to August 1998, he was with California PATH, University of California, Berkeley, leading the research team on longitudinal control systems for the Automated Highway Systems Program. He is currently Nelson Assistant Professor in the Department of Mechanical Engineering at the University of Minnesota. His active research interests include control design and state estimation for nonlinear systems, fault diagnostics, intelligent transportation systems, active noise control, and microelectromechanical systems (MEMS) sensor design. He has authored more than 35 refereed publications and received two patents.

Dr. Rajamani has won several awards including the CAREER award from the National Science Foundation, the 2001 Outstanding Paper award from the journal IEEE TRANSACTIONS ON CONTROL SYSTEMS TECHNOLOGY, the Distinguished Service Team Award from the University of California, Berkeley, and the Outstanding Achievement of the Year award from United Technologies Research Center.

Lee Alexander received the Bachelor of Mechanical Engineering degree from the University of Minnesota, Minneapolis, in 1996, and the M.S.M.E. degree from the same university in 1999.

Since 1999, he has been a Research Fellow in the Intelligent Vehicles Lab at the University of Minnesota. His research activities include GPS-based automatic control of vehicles, various drive assistive technologies, and the design of small commuter vehicles.